iScience

CellPress
OPEN ACCESS

Article

Native T_1 mapping-based radiomics diagnosis of kidney function and renal fibrosis in chronic kidney disease

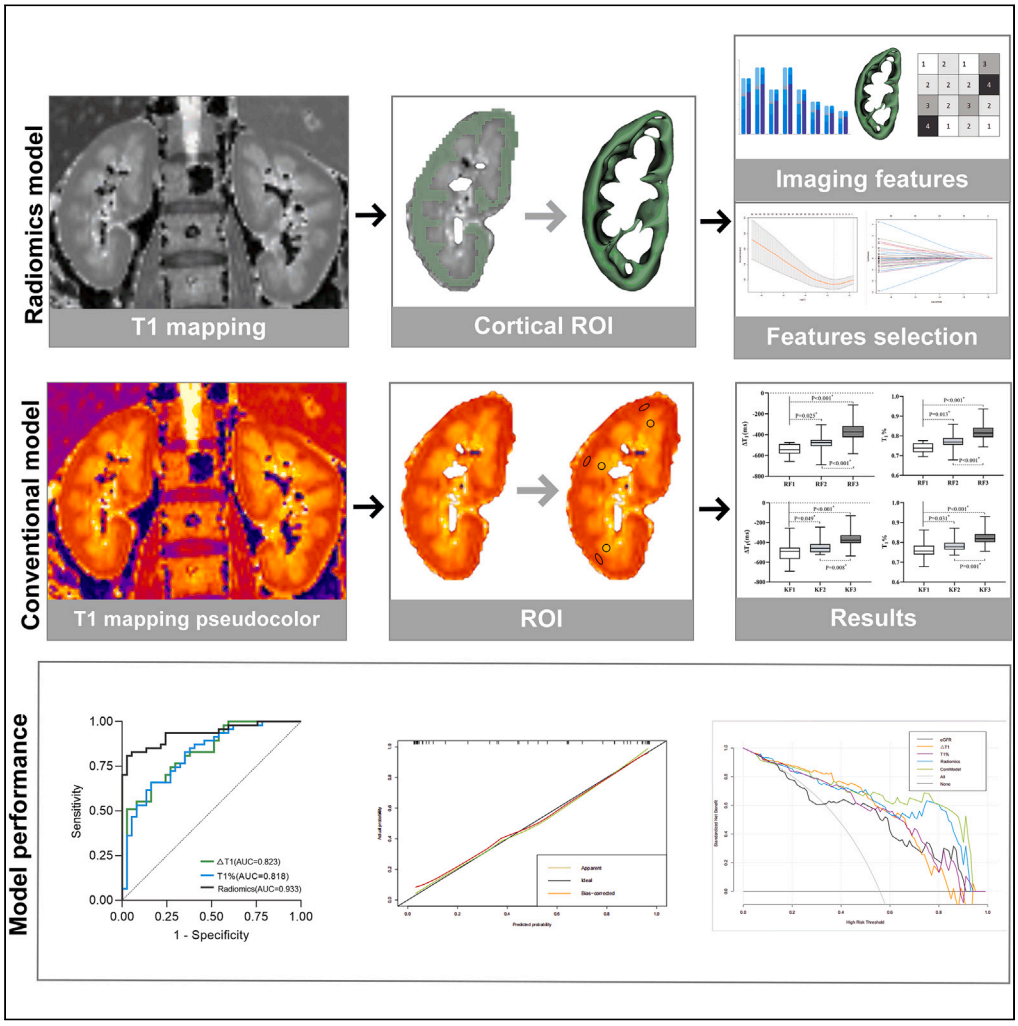

Chaogang Wei, Zhicheng Jin, Qing Ma, ..., Linsen Jiang, Kai Song, Zhen Jiang

jiangzhen0416@suda.edu.cn (Z.J.)
szjls@aliyun.com (L.J.)
songkaift3@live.cn (K.S.)

Highlights

Native T_1 mapping-based radiomics models can predict renal fibrosis in CKD patients

Native T_1 mapping-based radiomics models can identify renal function in CKD patients

Native T_1 mapping-based radiomics outperformed the conventional T_1 mapping parameters

Native T_1 mapping-based radiomics can provide more information for CKD management

Wei et al., iScience 27, 110493
August 16, 2024
https://doi.org/10.1016/j.isci.2024.110493

iScience

CellPress
OPEN ACCESS

Article

Native T_1 mapping-based radiomics diagnosis of kidney function and renal fibrosis in chronic kidney disease

Chaogang Wei,[1,5] Zhicheng Jin,[2,5] Qing Ma,[1,5] Yilin Xu,[3] Ye Zhu,[3] Ying Zeng,[3] Rui Zhang,[4] Yueyue Zhang,[1] Linsen Jiang,[3,*] Kai Song,[3,*] and Zhen Jiang[1,6,*]

SUMMARY

Chronic kidney disease (CKD) raises major concerns for global public health as it is characterized by high prevalence, low awareness, high healthcare costs, and poor prognosis. Therefore, our study prospectively established and validated native T_1 mapping-based radiomics models for the prediction of renal fibrosis and renal function in patients with CKD. Moreover, the area under the receiver operating characteristic curve (AUC) and diagnostic sensitivity, specificity, accuracy, positive predictive value, and negative predictive value were used to evaluate its performance. Thus, our results show that radiomics based on native T_1 mapping images can better identify renal function and renal fibrosis in patients with CKD and outperform conventional T_1 mapping parameters of ΔT_1 and T_1%, thus providing more information for CKD management and clinical decision-making.

INTRODUCTION

Chronic kidney disease (CKD) refers to a variety of conditions arising from abnormal kidney structure or function that persist for more than three months and have health implications.[1] CKD has become a major global public health problem characterized by high prevalence, low awareness, high medical costs, and poor prognosis.[2] Accurately monitoring of kidney function (KF), disease progression, and response to treatment can improve outcomes and prognosis of patients with CKD. The estimated glomerular filtration rate (eGFR) is the most commonly used clinical index to evaluate KF, its decline is considered to be a loss or failure of KF and continues to guide clinical management.[3] However, the serum creatinine (Scr)-based eGFR has high variability with susceptible to creatinine levels.[4] In addition, it cannot accurately reflect split renal function, which is often required for the preoperative evaluation for patients with kidney disease.[5]

More importantly, renal fibrosis (RF) inevitably develops as CKD progresses. As the hallmark of CKD, the severity of RF tends to be closely correlated with the prognosis of CKD.[6,7] Percutaneous renal biopsy remains the gold standard for the diagnosis of RF. However, the invasive procedure is associated with biopsy-related sampling errors and an increased risk of complications, such as infection, bleeding, hematuria, or hematoma.[8] As a non-invasive diagnostic tool, magnetic resonance imaging (MRI) plays a positive role in the management of kidney disease, including CKD.[9,10] Continuous researches have focused on the use of functional MRIs in the assessment of CKD, including diffusion-weighted imaging (DWI),[11] magnetic resonance elastography (MRE),[12] blood oxygenation level-dependent (BOLD) MRI,[13] arterial spin labeling (ASL),[14] and quantitative T_1, T_2, or T_2* mapping,[15] which have revealed the pathophysiological characteristics of renal interstitial diffusion, elasticity changes, oxygenation, microvascular perfusion, and tissue inherent relaxation. Native T_1 mapping provides the quantification of renal tissue T_1 values on a pixel-by-pixel basis, without the need for gadolinium.[16] In previous studies, we have confirmed the value of native T_1 mapping for diagnosis of KF and RF in patients with CKD.[17] However, the region of interest (ROI) of the native T_1 mapping sequence was delineated at only a few locations on a single slice image, making it time consuming, subjective, unrepeatable, and difficult to accurately represent the actual state of the kidney.

Artificial intelligence-driven radiomics for medical imaging analysis may be a good solution. Radiomics provides high-throughput feature extraction from medical images for quantitative analysis and prediction of various clinical endpoints.[18] Several studies have demonstrated the potential of radiomics as a non-invasive, personalized medicine tool, with promising performance in tumor diagnosis, treatment response monitoring, and prognosis.[19] Previous studies have confirmed the feasibility of using radiomics based on conventional T_2-weighted imaging (T2WI) or functional MRI sequences (such as DWI and BOLD) to assess KF or RF in patients with CKD.[20] Only a limited number of studies have

[1]Department of Radiology, The Second Affiliated Hospital of Soochow University, Suzhou 215004, China
[2]Department of Nuclear Medicine, The Second Affiliated Hospital of Soochow University, Suzhou 215004, China
[3]Department of Nephrology, The Second Affiliated Hospital of Soochow University, Suzhou 215004, China
[4]Department of Radiology, Hulunbuir People's Hospital, Hulunbuir 021008, China
[5]These authors contributed equally
[6]Lead contact
*Correspondence: jiangzhen0416@suda.edu.cn (Z.J.), szjls@aliyun.com (L.J.), songkaift3@live.cn (K.S.)
https://doi.org/10.1016/j.isci.2024.110493

investigated the potential of using native T_1 mapping-based radiomics in the management of CKD.[21,22] However, small sample size and lack of detailed verification made it difficult to obtain repeatability and reliability of the results. Native T_1 mapping images can be used to differentiate the renal cortex and medulla.[23] In previous studies, the ROI delineation was based on the whole kidney, not the renal cortex or medulla. The segmentation of renal cortical tissues was helpful in obtaining more accurate radiomic results because almost all renal biopsy specimens were taken from the renal cortex and RF has greater effects on the renal cortex.[24,25] To our knowledge, we are the first to perform the renal cortical segmentation based on the native T_1 mapping images and then to evaluate the diagnostic value of radiomics based on the renal cortex in a prospective study with a relatively large sample size.

Hence, the aim of this study was to investigate the diagnostic accuracy of radiomics based on native T_1 mapping images to assess KF and RF in patients with CKD and compare it with the conventional T_1 mapping parameters.

RESULTS

Patient characteristics

The baseline characteristics of 120 patients with CKD, including 84 patients in the training cohort and 36 patients in the validation cohort are shown in Table 1. The flowchart with patient exclusion criteria is shown in Figure 1. These patients were further divided into three subgroups (KF 1, KF 2, and KF 3) according to CKD stage. In the training cohort, the normal (KF 1), mildly impaired (KF 2), and moderately to severely impaired (KF 3) kidney function groups included 37, 22, and 25 patients, respectively. In the validation cohort, there were 16 patients with KF 1, 10 patients with KF 2, and 10 patients with KF 3. Patient clinical information, including age, gender, height, weight, BMI, blood pressure, and blood glucose showed no significant difference between the three groups in the training and validation cohorts ($p > 0.05$). There were significant differences in the levels of eGFR, Scr, and BUN between the three groups in the training and validation cohorts ($p < 0.05$). The eGFR gradually decreased, while Scr and BUN gradually increased as the degree of KF increased. In addition, there was also a significant difference in the degree of RF between the three groups ($p < 0.05$). The proportion of patients with moderate-to-severe RF increased significantly as the degree of KF increased. In our study, a total of 11 diseases causing CKD were pathologically confirmed by renal biopsy. The main primary causes were IgA nephropathy and membranous nephropathy, which together accounted for almost 67% (80/120) of all cases.

Development of radiomics models

The cortical ROI was delineated using the native T_1 mapping image thresholding, as illustrated in Figure S1. We constructed four different radiomics models based on native T_1 mapping images to assess KF and RF in patients with CKD, including the persistence (KF 1 vs. KF 2 and KF 3, RF 1 vs. RF 2 and RF 3) and degree (KF 2 vs. KF 3 and RF 2 vs. RF3). To identify the persistence (KF 1 vs. KF 2 and KF 3) and degree (KF 2 vs. KF 3) of KF, we excluded these features with ICC less than 0.75 and extracted 798 and 765 features from native T_1 mapping images, respectively. Finally, based on the LASSO regression algorithm, 11 and 9 features were extracted (Figure S2). Similarly, to identify the persistence (RF 1 vs. RF 2 and RF 3) and degree (RF 2 vs. RF 3) of RF in patients with CKD, we finally extracted 7 and 6 features from native T_1 mapping images, respectively. All extracted features and their coefficients are detailed in Figure S3.

For conventional native T_1 mapping images analysis, the two radiologists had good reproducibility for all values of four T_1 mapping parameters for both kidneys, with ICCs greater than 0.75 and p values less than 0.001. The results of the interobserver agreement are shown in Table S1. Analyses were performed using the value from the right (biopsied) kidney, as there were no significant differences in the T_1 mapping parameters between the two kidneys (Figure S4). Among the four T_1 mapping parameters, ΔT_1 and T_1% were the most useful for identifying KF and RF in CKD patients, rather than T_1-C or T_1-M, in overall (Tables 2 and 3) and pairwise (Figures S5 and S6) comparisons in both the training and validation cohorts. Increased cortical T_1 resulted in a gradually reduced T_1 corticomedullary difference (ΔT_1) in the mild and moderate-to-severe RF (RF 2 and RF 3) when compared with no RF (RF 1), along with gradual increases in the T_1% (Figure 2).

To better identify RF in patients with CKD, we constructed the clinical-based model by selecting the optimal clinical indicator through univariate logistic analysis (Table S2) and comparing AUCs. We found that the eGFR with the highest AUC was the best for assessing RF, while Scr and BUN with smaller AUCs were excluded. In addition, we also constructed the combined model by incorporating the radiomics with the eGFR.

Comparisons of diagnostic performance between models

To identify KF in patients with CKD, we compared the diagnostic performance of three models, including the radiomics model, conventional T_1 mapping parameter-based models (the ΔT_1 and the T_1%), as shown in Tables 4, S3, and S4. In the comparison of normal and impaired KF (KF 1 vs. KF 2 and KF3), the AUC of the radiomics model was 0.933, greater than that of ΔT_1 (AUC = 0.823, $p = 0.021$) and T_1% (AUC = 0.818, $p = 0.012$) in the training cohort. The diagnostic sensitivity, specificity, and accuracy of the radiomics model were the highest at 0.809, 0.973, and 0.845. Similarly, the radiomics model achieved the best diagnostic performance with the highest AUC (0.891) and the highest accuracy (0.889) in the validation cohort. When comparing mildly with moderately to severely impaired KF (KF 2 vs. KF 3), we found that the radiomics model reached the highest AUC (AUC = 0.916) with the best diagnostic performance (specificity: 0.864; accuracy: 0.830) in the training cohort. Similar results were obtained in the validation cohort with the highest AUC of the radiomic model (AUC = 0.860).

As shown in Tables 4, S3, and S4, to identify RF in patients with CKD, we also compared five models, including the radiomics model, conventional T_1 mapping parameter-based models (the ΔT_1 and the T_1%), the clinically based model (the eGFR) and the combined model (radiomics+ eGFR). In the comparison of no RF and RF (RF 1 vs. RF 2 and RF 3), we found that the radiomic model had the highest AUC

Table 1. Baseline characteristics in patients with CKD

	Training cohort (n = 84)				Validation cohort (n = 36)			
	KF 1[a] (n = 37)	KF 2[b] (n = 22)	KF 3[c] (n = 25)	P_t	KF 1 (n = 16)	KF 2 (n = 10)	KF 3 (n = 10)	P_v
Age (year)	43 ± 15	49 ± 11	49 ± 16	0.201	43 ± 14	46 ± 11	49 ± 14	0.499
Gender (male, %)	16 (43.2%)	14 (63.6%)	11 (44.0%)	0.269	8 (50.0%)	7 (70.0%)	5 (50.0%)	0.549
Height (m)	1.65 ± 0.09	1.66 ± 0.08	1.66 ± 0.08	0.639	1.62 ± 0.10	1.68 ± 0.06	1.66 ± 0.09	0.243
Weight (kg)	66.47 ± 12.01	69.78 ± 14.22	68.44 ± 12.77	0.615	64.64 ± 12.83	66.95 ± 8.41	67.20 ± 10.68	0.810
BMI (kg/m^2)	24.49 ± 3.63	25.01 ± 3.53	24.75 ± 4.01	0.874	24.54 ± 3.09	23.77 ± 2.37	24.52 ± 3.67	0.805
Blood pressure (hypertension[d], %)	22 (59.5%)	15 (68.2%)	18 (72.0%)	0.567	9 (56.3%)	4 (40.0%)	6 (60.0%)	0.623
Blood glucose (mmol/L)	4.85 (4.42, 5.11)	4.72 (4.57, 5.07)	4.90 (4.38, 5.97)	0.974	4.78 ± 0.74	4.85 ± 0.53	4.61 (4.46, 4.71)	0.810
eGFR (mL/min/1.73m^2)	110.04 ± 14.36	77.37 ± 7.85	45.93 ± 10.25	<0.001*	114.73 ± 15.38	72.58 ± 6.47	40.31 ± 15.64	<0.001*
Scr (μmol/L)	62.78 ± 15.22	91.23 ± 16.91	128 (113, 146)	<0.001*	55.50 (50.80, 65.00)	99.70 ± 14.64	150.70 ± 73.74	<0.001*
BUN (mmol/L)	4.87 ± 1.62	6.34 ± 1.23	8.80 ± 2.47	<0.001*	3.85 (3.33, 4.80)	5.91 ± 1.72	8.31 ± 3.53	0.003*
24h-UPRO (g/24h)	2.86 (1.33, 5.73)	3.71 (2.23, 8.17)	2.30 (1.01, 4.99)	0.237	2.71 (1.57, 5.34)	1.45 (0.71, 2.24)	2.34 (1.12, 6.44)	0.196
RF stage				<0.001*				0.012*
1 (no, 0%)	15 (40.5%)	1 (4.5%)	0 (0.0%)		5 (31.2%)	0 (0.0%)	2 (20.0%)	
2 (mild, ≤25%)	20 (54.1%)	15 (68.2%)	5 (20.0%)		9 (56.3%)	4 (40.0%)	2 (20.0%)	
3 (moderate to severe, >25%)	2 (5.4%)	6 (27.3%)	20 (80.0%)		2 (12.5%)	6 (60.0%)	6 (60.0%)	
Pathological type of CKD				N.A.				N.A.
IgA nephropathy	10	7	7		5	7	3	
Membranous nephropathy	22	3	3		10	1	2	
Minimal change nephropathy	2	3	0		0	0	2	
Focal segmental glomerulosclerosis	0	2	6		0	1	1	
Hypertensive nephropathy	0	1	2		1	0	1	
Lupus nephritis	3	2	0		0	0	0	
Diabetic nephropathy	0	1	2		0	1	0	
Hepatitis B virus-related nephropathy	0	1	0		0	0	0	
Amyloid nephropathy	0	1	0		0	0	0	
Glomerular podocytes	0	0	2		0	0	0	
Tubulointerstitial nephritis	0	1	3		0	0	1	

CKD, chronic kidney disease; BMI, body mass index; eGFR, estimated glomerular filtration rate; Scr, serum creatinine; BUN, blood urea nitrogen; 24h-UPRO, 24-h urinary protein; RF, renal fibrosis; KF, kidney function.

[a]KF1: CKD G1 (eGFR≥90 mL/min/1.73m^2).

[b]KF2: CKD G2 (eGFR 60-89 mL/min/1.73m^2).

[c]KF3: CKD G3-5 (eGFR<60 mL/min/1.73m^2).

[d]Hypertension was defined as systolic/diastolic blood pressure ≥140/90 mmHg; values are mean with standard deviation or median with lower and upper quartile in parentheses or number with percentage in parentheses. P_t, p values in comparisons in the training cohort; P_v, p values in comparisons in the validation cohort; N.A., not applicable; *statistically significant.

of 0.929, slightly higher than that of the combined model (AUC = 0.927, p = 0.938), higher than that of ΔT_1 (AUC = 0.868, p = 0.165), T_1% (AUC = 0.886, p = 0.270), and eGFR (AUC = 0.829, p = 0.026) in the training cohort. Similar results were seen in the validation cohort with the highest AUCs for both the radiomic model and the combined model (both AUCs = 0.936). When comparing mild RF with

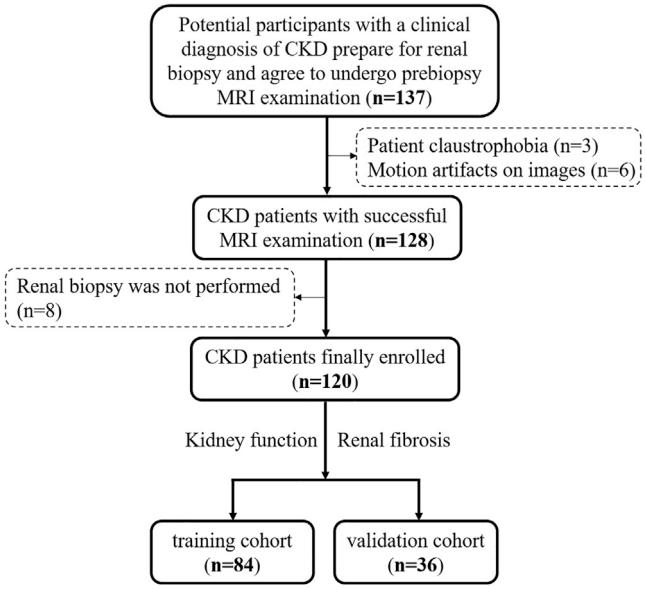

Figure 1. Flowchart with exclusion criteria

moderate-to-severe RF (RF 2 vs. RF 3), we found that the combined model achieved the highest AUC of 0.911, slightly higher than that of the radiomic model (AUC = 0.904, $p = 0.671$) and higher than that of ΔT_1 (AUC = 0.854, $p = 0.307$), T_1% (AUC = 0.852, $p = 0.229$), and eGFR (AUC = 0.801, $p = 0.025$) in the training cohort. However, in the validation cohort we found that the combined model had the highest AUC of 0.946, higher than that of eGFR (AUC = 0.912, $p = 0.365$), the radiomic model (AUC = 0.877, $p = 0.227$), ΔT_1 (AUC = 0.868, $p = 0.147$), and T_1% (AUC = 0.804, $p = 0.014$). Comparisons of AUCs between different models in the training and validation cohorts were illustrated in Figure 3, Tables S3 and S4.

Clinical application of radiomics models

The calibration and decision curve analysis were validated in the validation cohort, as shown in Figure 4. The calibration of models was internally performed by a calibration curve with bootstrap sampling. For the calibration curve, the curve of the diagnostic model was close to the ideal curve, indicating that the model had good fitting and prediction ability. The Brier scores of the radiomics model for KF persistence (KF 1 vs. KF 2 and KF 3) and KF degree (KF 2 vs. KF 3) were 0.106 and 0.108, respectively. The Brier scores of the radiomics model for RF persistence (RF 1 vs. RF 2 and RF 3) and RF degree (RF 2 vs. RF3) were 0.073 and 0.130, respectively. In terms of the clinical benefits, it is obvious from the decision curve that the radiomics model had better clinical benefits than conventional T_1 mapping parameter-based models (the ΔT_1 and the T_1%) in the evaluation of KF. Both the radiomics model and the combined model achieved similarly satisfactory clinical benefits for RF, better than conventional T_1 mapping parameter-based models (the ΔT_1 and the T_1%) and the clinically based model (the eGFR).

Table 2. Values of T_1 mapping for assessment of kidney function in CKD patients

T_1 mapping parameters	Training cohort (n = 84)				Validation cohort (n = 36)			
	KF 1[a] (n = 37)	KF 2[b] (n = 22)	KF 3[c] (n = 25)	P_t	KF 1 (n = 16)	KF 2 (n = 10)	KF 3 (n = 10)	P_v
T_1-C (ms)	1590.83 ± 106.92	1608.59 ± 112.09	1649.69 (1608.85, 1728.11)	0.010*	1598.91 ± 126.19	1619.37 ± 92.96	1651.53 (1646.95, 1677.09)	0.128
T_1-M (ms)	2099.40 ± 117.67	2054.64 ± 112.19	2046.14 ± 142.51	0.197	2121.04 ± 117.82	2028.38 ± 105.50	2066.15 ± 140.51	0.168
ΔT_1 (ms)	−508.57 ± 81.77	−459.20 (−496.67, −424.52)	−365.50 ± 87.02	<0.001*	−522.14 ± 58.04	−409.02 ± 58.85	−388.66 ± 132.79	0.001*
T_1%	0.7580 ± 0.0352	0.7828 ± 0.0321	0.8224 ± 0.0374	<0.001*	0.7533 ± 0.0291	0.7985 ± 0.0263	0.7907 (0.7760, 0.8359)	0.001*

[a]KF1: CKD G1 (eGFR ≥ 90 mL/min/1.73m^2).
[b]KF2: CKD G2 (eGFR 60-89 mL/min/1.73m^2).
[c]KF3: CKD G3-5 (eGFR<60 mL/min/1.73m^2); T_1-C, mean cortical T_1 value; T_1-M, mean medullary T_1 value; ΔT_1, mean corticomedullary difference; T_1%, mean corticomedullary ratio; P_t, p values in comparisons in the training cohort; P_v, p values in comparisons in the validation cohort; *, statistically significant.

Table 3. Values of T_1 mapping for assessment of renal fibrosis in CKD patients

T_1 mapping parameters	Training cohort (n = 84)				Validation cohort (n = 36)			
	RF 1[a] (n = 16)	RF 2[b] (n = 38)	RF 3[c] (n = 30)	P_t	RF 1 (n = 7)	RF 2 (n = 17)	RF 3 (n = 12)	P_v
T_1-C (ms)	1534.74 ± 82.13	1621.96 ± 125.17	1650.37 (1601.75, 1678.52)	0.001*	1615.48 ± 111.89	1630.21 ± 107.01	1660.11 ± 146.71	0.709
T_1-M (ms)	2077.24 ± 81.74	2104.85 ± 113.78	2019.62 ± 138.30	0.015*	2140.78 ± 124.62	2101.75 ± 106.45	2002.36 (1915.29, 2089.90)	0.084
ΔT_1 (ms)	−542.50 ± 50.69	−476.87 (−507.47, −451.27)	−363.52 ± 105.25	<0.001*	−525.29 ± 66.71	−471.54 ± 58.99	−372.51 ± 81.66	0.001*
T_1%	0.7387 ± 0.0233	0.7701 ± 0.0319	0.8219 ± 0.0447	<0.001*	0.7546 ± 0.0280	0.7832 (0.7432, 0.7984)	0.8167 ± 0.0369	0.002*

[a]RF1: no RF (0% renal fibrosis).
[b]RF2: mild RF (≤25% renal fibrosis).
[c]RF3: moderate to severe RF (>25% renal fibrosis); T_1-C, mean cortical T_1 value; T_1-M, mean medullary T_1 value; ΔT_1, mean corticomedullary difference; T_1%, mean corticomedullary ratio; P_t, p values in comparisons in the training cohort; P_v, p values in comparisons in the validation cohort; *, statistically significant.

DISCUSSION

In this study, we found that radiomics based on native T_1 mapping images could robustly and effectively evaluate KF and RF in patients with CKD. Previous studies on functional MRI sequences-based radiomics in the evaluation of CKD and RF have rarely been reported. Chen et al.[20] retrospectively applied the multimodal MRI texture model based on T2WI, DWI, and BOLD sequences to assess KF and RF in patients with diabetic nephropathy. However, fibrosis classification and pathological results were not reported in their studies. More importantly, the delineation of ROI was aimed at the whole kidney not the renal cortex. The delineation details were not clearly explained. In addition, the lack of validation reduced the reliability of their studies. Hua et al.[22] concluded that multiparametric MRI combining DWI and T_1 mapping could distinguish patients with CKD from controls and evaluate the severity of RF. However, their ROIs were still sketched by taking points at

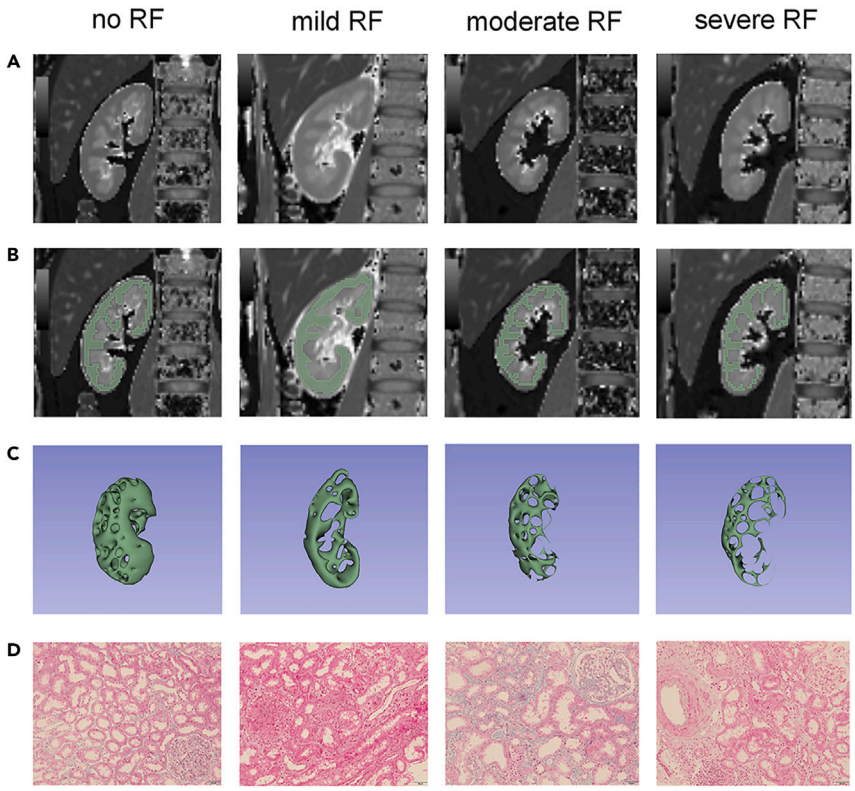

Figure 2. Comparison of native T_1 mapping images among patients with pathologically confirmed by RF 1 (no RF, 0% fibrosis), RF 2 (mild RF, ≤25% fibrosis), and RF 3 (moderate RF and severe RF, >25% fibrosis)

Table 4. Diagnostic performance comparisons of kidney function and renal fibrosis

	AUC (95%CI)	SEN	SPE	ACC	PPV	NPV
KF 1 vs. KF 2 and KF 3						
Training cohort						
Radiomics	0.933(0.856–0.976)	0.809	0.973	0.845	0.830	0.865
ΔT_1	0.823(0.725–0.898)	0.660	0.838	0.726	0.766	0.676
T_1%	0.818(0.719–0.894)	0.660	0.838	0.738	0.766	0.703
Validation cohort						
Radiomics	0.891(0.742–0.970)	0.850	0.937	0.889	0.850	0.938
ΔT_1	0.881(0.730–0.965)	0.850	0.750	0.806	0.850	0.750
T_1%	0.859(0.703–0.952)	0.900	0.688	0.750	0.800	0.688
KF 2 *vs.* KF 3						
Training cohort						
Radiomics	0.916(0.798–0.977)	0.840	0.864	0.830	0.840	0.818
ΔT_1	0.798(0.656–0.901)	0.800	0.818	0.766	0.800	0.727
T_1%	0.809(0.668–0.909)	0.880	0.727	0.787	0.800	0.773
Validation cohort						
Radiomics	0.860(0.633–0.972)	0.800	0.900	0.800	0.800	0.800
ΔT_1	0.520(0.289–0.745)	0.400	0.900	0.550	0.400	0.700
T_1%	0.510(0.280–0.736)	0.700	0.000	0.500	0.400	0.600
RF 1 vs. RF 2 and RF 3						
Training cohort						
Radiomics	0.929(0.854–0.974)	0.818	0.912	0.905	0.971	0.625
ΔT_1	0.868(0.776–0.932)	0.721	0.938	0.833	0.956	0.313
T_1%	0.886(0.798–0.945)	0.735	0.938	0.845	0.956	0.375
eGFR	0.829(0.731–0.902)	0.938	0.735	0.810	0.926	0.313
Combined Model (Radiomics + eGFR)	0.927(0.849–0.973)	0.938	0.838	0.940	0.985	0.750
Validation cohort						
Radiomics	0.936(0.801–0.990)	1.000	0.857	0.972	1.000	0.857
ΔT_1	0.837(0.677–0.939)	0.759	0.857	0.833	0.966	0.286
T_1%	0.818(0.654–0.926)	0.552	1.000	0.889	1.000	0.429
eGFR	0.601(0.425–0.760)	0.857	0.413	1.000	1.000	1.000
Combined Model (Radiomics + eGFR)	0.936(0.801–0.990)	0.857	1.000	0.972	1.000	0.857
RF 2 *vs.* RF 3						
Training cohort						
Radiomics	0.904(0.808–0.962)	0.967	0.711	0.824	0.733	0.895
ΔT_1	0.854(0.748–0.928)	0.767	0.921	0.824	0.700	0.921
T_1%	0.852(0.745–0.926)	0.833	0.763	0.765	0.667	0.842
eGFR	0.801(0.686–0.888)	0.816	0.767	0.779	0.700	0.842
Combined Model (Radiomics + eGFR)	0.911(0.817–0.967)	0.763	0.967	0.809	0.733	0.868
Validation cohort						
Radiomics	0.877(0.702–0.969)	0.667	1.000	0.724	0.667	0.765
ΔT_1	0.868(0.690–0.964)	0.750	0.941	0.828	0.750	0.882
T_1%	0.804(0.615–0.927)	0.583	0.941	0.724	0.667	0.765
eGFR	0.912(0.746–0.985)	0.824	0.833	0.793	0.750	0.824
Combined Model (Radiomics + eGFR)	0.946(0.794–0.996)	0.824	1.000	0.862	0.833	0.882

AUC, area under the receiver operating characteristic curve; SEN, sensitivity; SPE, specificity; ACC, accuracy; PPV, positive predictive value; NPV, negative predictive value; KF, kidney function; KF 1, CKD G1 (eGFR≥90 mL/min/1.73m^2); KF 2, CKD G2 (eGFR 60-89 mL/min/1.73m^2); KF 3, CKD G3-5 (eGFR<60 mL/min/1.73m^2); RF, renal fibrosis; RF 1, no RF (0% renal fibrosis); RF 2, mild RF (≤25% renal fibrosis); RF3, moderate-to-severe RF (>25% renal fibrosis); ΔT_1, mean corticomedullary difference; T_1%, mean corticomedullary ratio; eGFR, estimated glomerular filtration rate; the combined model, the combination of the radiomics and the eGFR; CI, confidence interval.

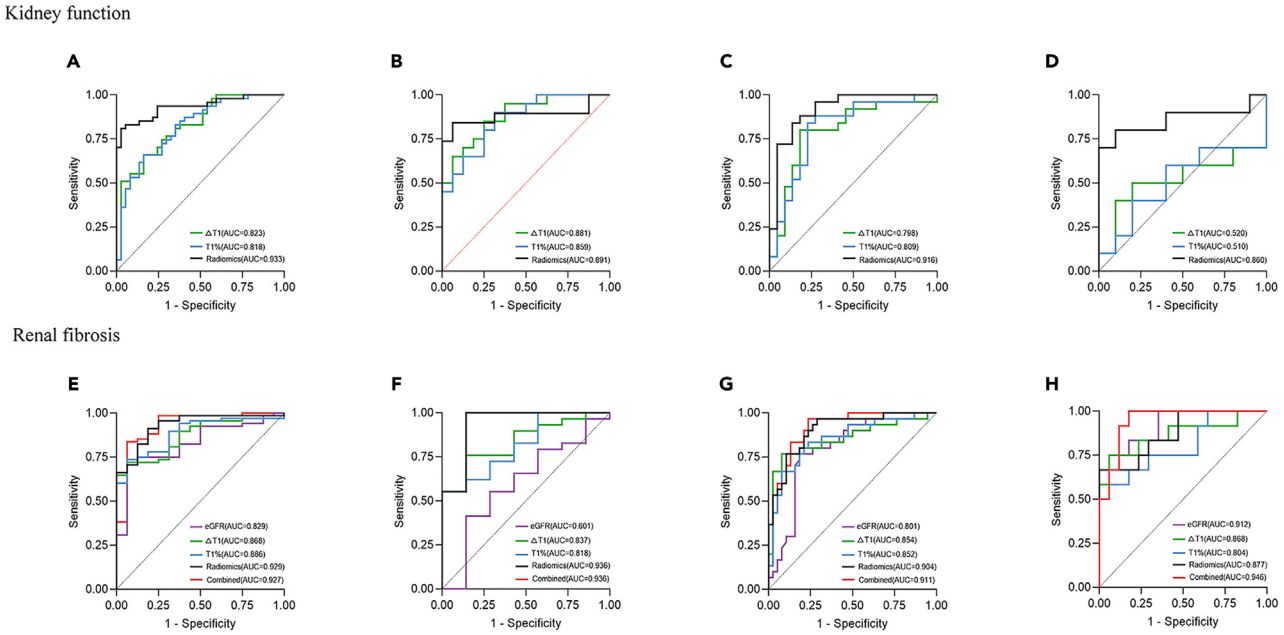

Figure 3. Diagnostic performance comparisons among different models for kidney function and renal fibrosis

(A–H) Receiver operating characteristic curve analyses for identifying the persistence (KF 1 vs. KF 2 and KF 3) and degree (KF 2 vs. KF 3) of kidney function in the training and validation cohorts (A–D), as well as the persistence (RF 1 vs. RF 2 and RF 3) and degree (RF 2 vs. RF 3) of kidney function in the training and validation cohorts (E–H).

different locations, instead of the entire cortex or medulla, which was easily susceptible to the operator's subjectivity. In addition, it had only 43 patients with pathological confirmation of CKD by renal biopsy in their studies, which is much smaller than the sample size (n = 120) in our study. Too small sample size and lack of validation make their results less accurate and reliable. Compared to previous studies, we sketched the cortical ROIs due to the facts that the vast majority of renal biopsies were taken from the renal cortex, which was more affected by RF. In our study, the native T_1 mapping images were generated based on the MOLLI sequence.[16] The good image quality allowed for clear identification of the renal cortex and medulla, which was a prerequisite for kidney segmentation and cortical ROI delineation. The imaging intensity (I) threshold was set within a specific range ($1150 < I < 1850$) and the entire cortical areas were then sketched slice by slice to ensure consistency among radiologists, making the ROI delineation more objective and less susceptible to operator subjectivity. Furthermore, our prospective study utilized a relatively large sample to analyze KF and RF in patients with CKD. Accurate ROI delineation and appropriate sample size were instrumental in producing more reliable research findings.

We also found that the radiomic model based on the native T_1 mapping images achieved robust and effective diagnostic performance in classifying KF and RF in patients with CKD. In the training and validation cohorts, the radiomics model reached the highest AUC and diagnostic accuracy for the identification of normal and impaired kidney function (KF 1 vs. KF 2 and KF 3). Similarly, with the highest AUC and accuracy, the radiomic model was effective in identifying mildly and moderately to severely impaired kidney function (KF 2 vs. KF 3). In the identification of no RF and RF (RF 1 vs. RF 2 and RF 3), we found that the radiomics model had the highest AUC, indicating that the radiomics model can identify the persistence of RF in patients with CKD. In identifying mild RF and moderate-to-severe RF (RF 2 vs. RF 3), the radiomics model achieved good diagnostic performance with high AUC, sensitivity, and accuracy in the training cohort. However, in the validation cohort, the radiomics model did not perform unsatisfactorily. This may be due to the selection bias caused by the small sample size in the validation cohort leading to a higher AUC value of the eGFR and the combined model, making the radiomics model not as good in comparison. In the evaluation of RF, we also observed that the combined model integrating radiomics and eGFR did not significantly improve diagnostic performance over the radiomics model, suggesting that the radiomics model alone has diagnostic advantages for KF and RF in patients with CKD. The diagnostic superiority of the radiomics for the assessment of KF or RF in patients with CKD was similarly shown in previous studies.[20,22]

In our study, among the four conventional native T_1 mapping parameters, the mean corticomedullary difference (ΔT_1) and the mean corticomedullary ratio (T_1%) showed better diagnostic performance than the mean cortical T_1 value (T_1-C) and the mean medullary T_1 value (T_1-M), which was similar to the study reported by Berchtold et al.[26] Although RF typically affects the renal cortex, the T_1-C value varied widely among individuals, the ΔT_1 and T_1% values generated by comparing the cortex with the medulla may reduce the difference. However, these values were obtained by manually delineating ROIs at only a few locations on a single slice image, making it time consuming, subjective, unrepeatable, and inaccurate. By setting image thresholds and sketching the ROI layer by layer, the ROI delineation of the radiomics model became simpler, more objective and more reliable, which was incomparable to conventional T_1 mapping parameters.[21] Our results showed that the radiomic model outperformed the ΔT_1 and the T_1% models in terms of diagnostic accuracy, as evidenced by a higher AUC. This

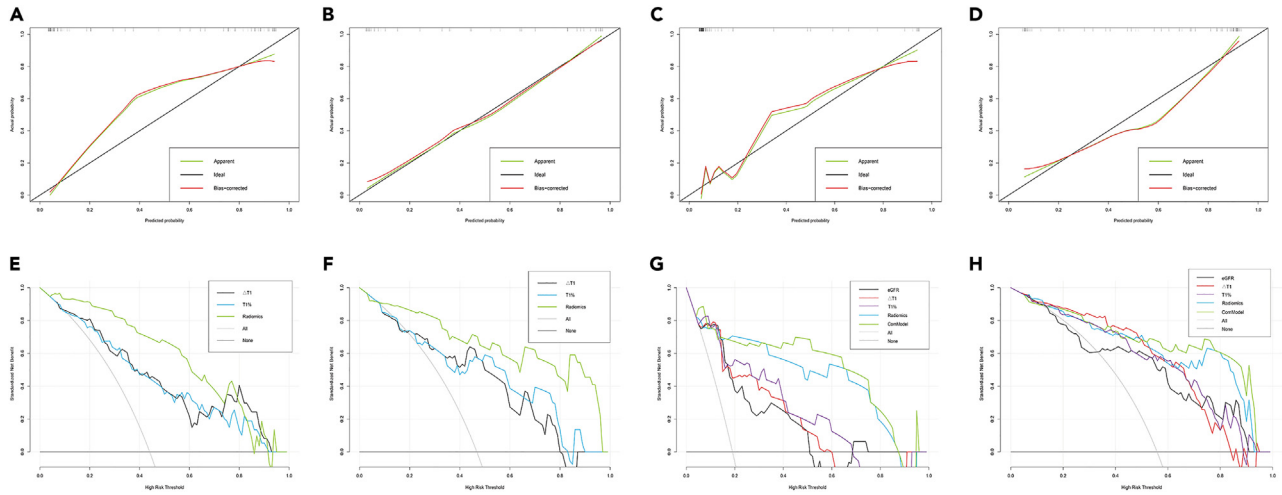

Figure 4. Validation of radiomics models for kidney function and renal fibrosis

(A–D) showed the calibration curves of different radiomics models for identifying the persistence (KF 1 vs. KF 2 and KF 3) and degree (KF 2 vs. KF 3) of kidney function, as well as the persistence (RF 1 vs. RF 2 and RF 3) and degree (RF 2 vs. RF 3) of kidney function. The Brier scores were 0.106, 0.108, 0.073, and 0.130, respectively. (E–H) compared the clinical benefits of these models for identifying KF and RF.

suggests that radiomics could improve the assessment of KF and RF in patients with CKD. In addition, we internally validated the radiomic model in the validation cohort of our study. We found that the radiomics model based on the native T_1 mapping images performed well and provided satisfactory clinical benefits in the calibration and decision curve analysis. This further demonstrates the reliability of radiomics in evaluating KF and RF in patients with CKD.

In addition to MRI, other non-invasive diagnostic tools, such as ultrasound, can also be used to assess renal structure, renal function, or renal fibrosis. However, ultrasound is a highly subjective examination that is influenced by the experience and perspective of the examiner. Compared with other ultrasound techniques, ultrasound elastography was employed to investigate kidney fibrosis by quantitative measurement of tissue stiffness. Nevertheless, the results relating to the applicability of ultrasound elastography in the measurement of kidney fibrosis were found to be inconsistent due to technical and anatomic limitations.[27] Studies have found that renal stiffness was only associated with medullary fibrosis, not with cortical fibrosis.[28] In recent years, ultrasound-based radiomics have been applied for the detection of fibrosis in patients with CKD. Ge et al.[29] incorporated radiomics feature derived from two-dimensional ultrasound and sound touch elastography with clinical features (age and eGFR) to improve the prediction of the severities of kidney fibrosis. In their studies, the ROI delineation was also limited to the renal cortex. In comparison to ultrasonic images, the native T_1 mapping images in our study demonstrated enhanced ability to distinguish between the cortex and medulla, which was crucial for accurate imaging segmentation and ROI delineation. Bandara et al.[30] employed radiomics features derived from ultrasound images to successfully identify CKD and healthy subjects. In their study, only 75 patients with CKD were recruited and 465 radiomics features were extracted, whereas in our study, a larger sample size (n = 120) and 851 features were performed.

In conclusion, the radiomics model based on native T_1 mapping images exhibited robust and satisfactory diagnostic performance for the assessment of kidney function and renal fibrosis in patients with CKD, which was superior to conventional T_1 mapping parameters of ΔT_1 and T_1%.

Limitations of the study

There are several limitations to our study. First, this is a prospective study conducted in a single center. Although the sample size in our study was relatively large compared to other relevant studies, a larger sample size from multi-centers will be recruited to validate our results in further studies. Second, we extracted only partial data from this group to internally validate the model. An external validation cohort should be included in the future to test the robustness of our model. Third, we constructed the radiomics model based only on the native T_1 mapping sequence, without the inclusion of the combined model of multiple MRI sequences. In this study, we only perform in-depth analysis for radiomics based on the native T_1 mapping sequence and compare it with conventional T_1 mapping parameters. Multi-sequence analysis in combination with other MRI sequences (DWI, T2* mapping) is under investigation in future studies.

STAR★METHODS

Detailed methods are provided in the online version of this paper and include the following:

- KEY RESOURCES TABLE
- RESOURCE AVAILABILITY

- Lead contact
- Materials availability
- Data and code availability
- EXPERIMENTAL MODEL AND STUDY PARTICIPANT DETAILS
  - Ethics statement
  - Patients
- METHOD DETAILS
  - Magnetic resonance imaging protocol
  - Kidney segmentation and ROI delineation
  - Conventional native T_1 mapping imaging analysis
  - Radiomics feature extraction
  - Radiomics feature selection and model construction
  - Models comparison and validation
  - Clinical and laboratory parameters
  - Renal histopathological evaluation
- QUANTIFICATION AND STATISTICAL ANALYSIS

SUPPLEMENTAL INFORMATION

Supplemental information can be found online at https://doi.org/10.1016/j.isci.2024.110493.

ACKNOWLEDGMENTS

This study was financially supported by the National Natural Science Foundation of China (grant no. 81801754), the Suzhou Youth Science and Technology Project (grant no. KJXW2023022), the Suzhou Science and Technology Bureau Key Technique Research Project (grant no. SKY2021046), and the Suzhou Science and Technology Bureau Development Plan Project (grant no. SLT2023031).

AUTHOR CONTRIBUTIONS

C.W.: conception and design, manuscript writing; Z. Jin: conception and design, data analysis; Q.M.: data analysis and interpretation; Y.X.: provision of study materials or patients; Y. Zhu: collection and assembly of data; Y. Zeng: administrative support; R.Z.: data analysis and interpretation; Y. Zhang: data analysis and interpretation; L.J.: conception and design; K.S.: administrative support; Z.J.: administrative support

DECLARATION OF INTERESTS

The authors declare no competing interests.

Received: February 1, 2024
Revised: April 26, 2024
Accepted: July 9, 2024
Published: July 14, 2024

REFERENCES

1. Levin, A., Stevens, P.E., Bilous, R.W., Coresh, J., and Winearls, C.G. (2013). Kidney disease: Improving global outcomes (KDIGO) CKD work group. KDIGO 2012 clinical practice guideline for the evaluation and management of chronic kidney disease. Kidney Int. Suppl. *3*, 1–150.
2. GBD Chronic Kidney Disease Collaboration (2020). Global, regional, and national burden of chronic kidney disease, 1990-2017: a systematic analysis for the Global Burden of Disease Study 2017. Lancet (London, England) *395*, 709–733. https://doi.org/10.1016/S0140-6736(20)30045-3.
3. Levey, A.S., Stevens, L.A., Schmid, C.H., Zhang, Y.L., Castro, A.F., Feldman, H.I., Kusek, J.W., Eggers, P., Van Lente, F., Greene, T., et al. (2009). A new equation to estimate glomerular filtration rate. Ann. Intern. Med. *150*, 604–612.
4. Porrini, E., Ruggenenti, P., Luis-Lima, S., Carrara, F., Jiménez, A., de Vries, A.P.J., Torres, A., Gaspari, F., and Remuzzi, G. (2019). Estimated GFR: time for a critical appraisal. Nat. Rev. Nephrol. *15*, 177–190. https://doi.org/10.1038/s41581-018-0080-9.
5. Shi, W., Liang, X., Wu, N., Zhang, H., Yuan, X., and Tan, Y. (2020). Assessment of Split Renal Function Using a Combination of Contrast-Enhanced CT and Serum Creatinine Values for Glomerular Filtration Rate Estimation. AJR Am. J. Roentgenol. *215*, 142–147. https://doi.org/10.2214/AJR.19.22125.
6. Humphreys, B.D. (2018). Mechanisms of Renal Fibrosis. Annu. Rev. Physiol. *80*, 309–326. https://doi.org/10.1146/annurev-physiol-022516-034227.
7. Liu, Y. (2011). Cellular and molecular mechanisms of renal fibrosis. Nat. Rev. Nephrol. *7*, 684–696. https://doi.org/10.1038/nrneph.2011.149.
8. Luciano, R.L., and Moeckel, G.W. (2019). Update on the Native Kidney Biopsy: Core Curriculum 2019. Am. J. Kidney Dis. *73*, 404–415. https://doi.org/10.1053/j.ajkd.2018.10.011.
9. Leung, G., Kirpalani, A., Szeto, S.G., Deeb, M., Foltz, W., Simmons, C.A., and Yuen, D.A. (2017). Could MRI Be Used To Image Kidney Fibrosis? A Review of Recent Advances and Remaining Barriers. Clin. J. Am. Soc. Nephrol. *12*, 1019–1028. https://doi.org/10.2215/CJN.07900716.
10. Morrell, G.R., Zhang, J.L., and Lee, V.S. (2017). Magnetic Resonance Imaging of the Fibrotic Kidney. J. Am. Soc. Nephrol. *28*, 2564–2570. https://doi.org/10.1681/ASN.2016101089.
11. Berchtold, L., Crowe, L.A., Combescure, C., Kassaï, M., Aslam, I., Legouis, D., Moll, S., Martin, P.Y., de Seigneux, S., and Vallée, J.P. (2022). Diffusion-magnetic resonance imaging predicts decline of kidney function in chronic kidney disease and in patients with a kidney allograft. Kidney Int. *101*, 804–813. https://doi.org/10.1016/j.kint.2021.12.014.

12. Han, J.H., Ahn, J.H., and Kim, J.S. (2020). Magnetic resonance elastography for evaluation of renal parenchyma in chronic kidney disease: a pilot study. Radiol. Med. *125*, 1209–1215. https://doi.org/10.1007/s11547-020-01210-1.
13. Li, C., Liu, H., Li, X., Zhou, L., Wang, R., and Zhang, Y. (2019). Application of BOLD-MRI in the classification of renal function in chronic kidney disease. Abdom. Radiol. *44*, 604–611. https://doi.org/10.1007/s00261-018-1750-6.
14. Li, L.P., Tan, H., Thacker, J.M., Li, W., Zhou, Y., Kohn, O., Sprague, S.M., and Prasad, P.V. (2017). Evaluation of Renal Blood Flow in Chronic Kidney Disease Using Arterial Spin Labeling Perfusion Magnetic Resonance Imaging. Kidney Int. Rep. *2*, 36–43. https://doi.org/10.1016/j.ekir.2016.09.003.
15. Dekkers, I.A., de Boer, A., Sharma, K., Cox, E.F., Lamb, H.J., Buckley, D.L., Bane, O., Morris, D.M., Prasad, P.V., Semple, S.I.K., et al. (2020). Consensus-based technical recommendations for clinical translation of renal T1 and T2 mapping MRI. Magma *33*, 163–176. https://doi.org/10.1007/s10334-019-00797-5.
16. Dekkers, I.A., Paiman, E.H.M., de Vries, A.P.J., and Lamb, H.J. (2019). Reproducibility of native T1 mapping for renal tissue characterization at 3T. J. Magn. Reson. Imaging. *49*, 588–596. https://doi.org/10.1002/jmri.26207.
17. Wei, C.G., Zeng, Y., Zhang, R., Zhu, Y., Tu, J., Pan, P., Ma, Q., Wei, L.Y., Zhao, W.L., and Shen, J.K. (2023). Native T1 mapping for non-invasive quantitative evaluation of renal function and renal fibrosis in patients with chronic kidney disease. Quant. Imaging Med. Surg. *13*, 5058–5071. https://doi.org/10.21037/qims-22-1304.
18. van Timmeren, J.E., Cester, D., Tanadini-Lang, S., Alkadhi, H., and Baessler, B. (2020). Radiomics in medical imaging-"how-to" guide and critical reflection. Insights Imaging *11*, 91. https://doi.org/10.1186/s13244-020-00887-2.
19. Zhang, Y.P., Zhang, X.Y., Cheng, Y.T., Li, B., Teng, X.Z., Zhang, J., Lam, S., Zhou, T., Ma, Z.R., Sheng, J.B., et al. (2023). Artificial intelligence-driven radiomics study in cancer: the role of feature engineering and modeling. Mil. Med. Res. *10*, 22. https://doi.org/10.1186/s40779-023-00458-8.
20. Chen, W., Zhang, L., Cai, G., Zhang, B., Lian, Z., Li, J., Wang, W., Zhang, Y., and Mo, X. (2023). Machine learning-based multimodal MRI texture analysis for assessing renal function and fibrosis in diabetic nephropathy: a retrospective study. Front. Endocrinol. *14*, 1050078. https://doi.org/10.3389/fendo.2023.1050078.
21. Aslam, I., Aamir, F., Kassai, M., Crowe, L.A., Poletti, P.A., Seigneux, S.d., Moll, S., Berchtold, L., and Vallée, J.P. (2023). Validation of automatically measured T1 map cortico-medullary difference (ΔT1) for eGFR and fibrosis assessment in allograft kidneys. PLoS One *18*, e0277277. https://doi.org/10.1371/journal.pone.0277277.
22. Hua, C., Qiu, L., Zhou, L., Zhuang, Y., Cai, T., Xu, B., Hao, S., Fang, X., Wang, L., and Jiang, H. (2023). Value of multiparametric magnetic resonance imaging for evaluating chronic kidney disease and renal fibrosis. Eur. Radiol. *33*, 5211–5221. https://doi.org/10.1007/s00330-023-09674-1.
23. de Bazelaire, C.M.J., Duhamel, G.D., Rofsky, N.M., and Alsop, D.C. (2004). MR imaging relaxation times of abdominal and pelvic tissues measured in vivo at 3.0 T: preliminary results. Radiology *230*, 652–659. https://doi.org/10.1148/radiol.2303021331.
24. Uppot, R.N., Harisinghani, M.G., and Gervais, D.A. (2010). Imaging-guided percutaneous renal biopsy: rationale and approach. AJR Am. J. Roentgenol. *194*, 1443–1449. https://doi.org/10.2214/AJR.10.4427.
25. Farris, A.B., Chan, S., Climenhaga, J., Adam, B., Bellamy, C.O.C., Serón, D., Colvin, R.B., Reeve, J., and Mengel, M. (2014). Banff fibrosis study: multicenter visual assessment and computerized analysis of interstitial fibrosis in kidney biopsies. Am. J. Transplant. *14*, 897–907. https://doi.org/10.1111/ajt.12641.
26. Berchtold, L., Friedli, I., Crowe, L.A., Martinez, C., Moll, S., Hadaya, K., de Perrot, T., Combescure, C., Martin, P.Y., Vallée, J.P., and de Seigneux, S. (2020). Validation of the corticomedullary difference in magnetic resonance imaging-derived apparent diffusion coefficient for kidney fibrosis detection: a cross-sectional study. Nephrol. Dial. Transplant. *35*, 937–945. https://doi.org/10.1093/ndt/gfy389.
27. Srivastava, A., Tomar, B., Prajapati, S., Gaikwad, A.B., and Mulay, S.R. (2021). Advanced non-invasive diagnostic techniques for visualization and estimation of kidney fibrosis. Drug Discov. Today *26*, 2053–2063. https://doi.org/10.1016/j.drudis.2021.02.016.
28. Early, H.M., Cheang, E.C., Aguilera, J.M., Hirschbein, J.S.W., Fananapazir, G., Wilson, M.D., and McGahan, J.P. (2018). Utility of Shear Wave Elastography for Assessing Allograft Fibrosis in Renal Transplant Recipients: A Pilot Study. J. Ultrasound Med. *37*, 1455–1465. https://doi.org/10.1002/jum.14487.
29. Ge, X.Y., Lan, Z.K., Lan, Q.Q., Lin, H.S., Wang, G.D., and Chen, J. (2023). Diagnostic accuracy of ultrasound-based multimodal radiomics modeling for fibrosis detection in chronic kidney disease. Eur. Radiol. *33*, 2386–2398. https://doi.org/10.1007/s00330-022-09268-3.
30. Bandara, M.S., Gurunayaka, B., Lakraj, G., Pallewatte, A., Siribaddana, S., and Wansapura, J. (2022). Ultrasound Based Radiomics Features of Chronic Kidney Disease. Acad. Radiol. *29*, 229–235. https://doi.org/10.1016/j.acra.2021.01.006.
31. Stevens, P.E., and Levin, A.; the Kidney Disease: Improving Global Outcomes Chronic Kidney Disease Guideline Development Work Group Members (2013). Evaluation and management of chronic kidney disease: synopsis of the kidney disease: improving global outcomes 2012 clinical practice guideline. Ann. Intern. Med. *158*, 825–830.
32. Zollner, F.G., Kocinski, M., Hansen, L., Golla, A.K., Rogelj, P., Lundervold, A., Materka, A., and Rogelj, P. (2021). Kidney Segmentation in Renal Magnetic Resonance Imaging-Current Status and Prospects. IEEE Access *9*, 71577–71605. https://doi.org/10.1109/ACCESS.2021.3078430.
33. Xu, J., Wu, X., Xu, Y., Ren, H., Wang, W., Chen, W., Shen, P., Li, X., Shi, H., Xie, J., et al. (2020). Acute Kidney Disease Increases the Risk of Post-Kidney Biopsy Bleeding Complications. Kidney Blood Press. Res. *45*, 873–882. https://doi.org/10.1159/000509443.
34. Srivastava, A., Palsson, R., Kaze, A.D., Chen, M.E., Palacios, P., Sabbisetti, V., Betensky, R.A., Steinman, T.I., Thadhani, R.I., McMahon, G.M., et al. (2018). The Prognostic Value of Histopathologic Lesions in Native Kidney Biopsy Specimens: Results from the Boston Kidney Biopsy Cohort Study. J. Am. Soc. Nephrol. *29*, 2213–2224. https://doi.org/10.1681/ASN.2017121260.

STAR★METHODS

KEY RESOURCES TABLE

REAGENT or RESOURCE	SOURCE	IDENTIFIER
Deposited data		
clinical data of patients	Department of Nephrology, The Second Affiliated Hospital of Soochow University	N/A
Magnetic Resonance Imaging	Department of Radiology, The Second Affiliated Hospital of Soochow University	N/A
Code for models	This paper	https://github.com/jzc0307/Renal-fibrosis.git
Software and algorithms		
R 4.1.1	R Development Core Team	https://cran.r-project.org/
Python 3.9.1	Python Development Core Team	https://www.python.org/
3D Slicer 5.0.3	3D Slicer Development Core Team	https://www.slicer.org/
SPSS 22.0	Stanford University	https://www.ibm.com/products/spss-statistics
MedCalc 15.2.2	AcadTechs company	https://medcalc.acadtechs.com/
GraphPad Prism 8	GraphPad company	http://www.graphpad-prism.cn

RESOURCE AVAILABILITY

Lead contact

Further information and requests for resources and reagents should be directed to and will be fulfilled by the lead contact, Zhen Jiang (jiangzhen0416@suda.edu.cn).

Materials availability

This study did not generate new unique reagents.

Data and code availability

- The radiological images and clinical data are available from the lead contact upon reasonable request.
- All original code has been deposited at the Github and is publicly available as of the date of publication. DOI is listed in the key resources table.
- Any additional information required to reanalyze the data reported in this paper is available from the lead contact upon request.

EXPERIMENTAL MODEL AND STUDY PARTICIPANT DETAILS

Ethics statement

This prospective, single-center study was approved by the Ethics Committee of our tertiary care institution (No. JD-LK-2022-060-01). Informed consent was obtained from all patients.

Patients

In the primary cohort, 137 consecutive patients who were clinically diagnosed with CKD in the nephrology department of our institution between October 2021 and August 2023 were recruited into the study, and ruled out other diseases including acute kidney injury (AKI), autosomal dominant polycystic kidney disease (ADPKD), etc. Patients with clinical diagnosis of CKD underwent renal MRI examination within 5 days (2.9 $\pm$ 1.0). Renal biopsy was performed within 3 days (2.1 $\pm$ 0.6) after MRI examination. The patient inclusion criteria were as follows: (1) age greater than 18 years, regardless of ethnicity and compliance with a clinical diagnosis of CKD based on the KDIGO 2012 guidelines,[31] mainly including albuminuria and/or urinary sediment abnormalities and/or decreased eGFR levels over three months. (2) Patients were prepared for renal biopsy. (3) MRI examination was performed within three days prior to renal biopsy. (4) There were no contraindications to the MRI scan. However, 17 patients were excluded in the following conditions: (1) inability to complete MRI examination due to claustrophobia (n = 3); (2) unsatisfactory quality of the MR images available for analysis (n = 6); (3) renal biopsy not finally performed (n = 8). Finally, a total of 120 patients with CKD were enrolled in the study and were analyzed from the KF and RF. These patients were then randomly assigned to the training cohort (n = 84) and the validation cohort (n = 36) in a 7:3 ratio.

METHOD DETAILS

Magnetic resonance imaging protocol

MRI was performed on both kidneys using a Prisma 3.0 Tesla MRI scanner (Siemens AG, Erlangen, Germany) with an 18-channel total imaging matrix body coil. Native T_1 mapping was acquired using an end-expiratory, electrocardiographically (ECG)-gated modified look-locker inversion recovery (MOLLI) sequence 5(3)3.[16] Breath holds were used to compensate for respiratory motion. The MOLLI images of both kidneys were acquired in the coronal plane. The parameters of the native T_1 mapping MRI protocol were as follows: repetition time (TR), 546.64 ms; echo time (TE), 1.1 ms; slice thickness, 5 mm; number of slices, 5; field of view (FOV), 290 mm × 290 mm; matrix, 144 mm × 144 mm; flip angle, 35°; spatial resolution, 2 × 2 × 5 mm^3; initial inversion time (TI), 284 ms; TI increment, 80 ms; 10-s breath hold per time. The scan time of the native T_1 mapping MRI sequence was approximately 2 min 47 s.

Kidney segmentation and ROI delineation

For the radiomics analysis, kidney segmentation and ROI delineation were manually performed slice by slice on native T_1 mapping images by the two radiologists (J.Z.C. with 6 years of experience and M.Q. with 8 years of experience in the genitourinary system). For better separation from the renal medulla, the cortical ROI was delineated using the T_1 mapping image thresholding.[32] The renal cortex was extracted in the T_1 mapping-thresholded image ranging from the intensity $I > 1150$ and $I < 1850$ and it turned down to zero when the intensity $I \leq 1150$ and $I \geq 1850$, the two radiologists were permitted to make minor modifications within the above threshold range in certain circumstances. In this study, the ROI delineation of radiomics was only obtained from the renal cortex due to the fact that RF occurs predominantly in the renal cortex, and has a greater effect on the cortex than on the medulla. All radiomics features were extracted with an open-resource 3D Slicer software (version 5.0.3). The two radiologists draw the outlines of all ROIs strictly according to the same criteria. All delineated ROIs should include only areas of the renal cortex that lie on the outer contour of the kidney, avoiding renal cystic tissue, artifacts and major vessels. Any discrepancy between the two radiologists was resolved by consensus, any continuous disagreement was resolved by a third senior radiologists (J.Z. with 20 years of experience) who made the final determination of the cortical ROIs. There were no significant differences in T_1 mapping parameters between the left and right kidneys,[17] and ROI delineation was performed only in the right (biopsied) kidney. Finally, 120 cortical ROIs in the right kidney were identified.

Conventional native T_1 mapping imaging analysis

All native T_1 mapping images were performed in the reconstruction software of the Siemens post-processing workstation (Syngo.via). For conventional native T_1 mapping image analysis, each image was independently analyzed by two other radiologists with 8 and 10 years of experience in renal MRI (Z.R. and Z.Y.Y.), who were blinded to pathological results and clinical information. Cortical and medullary ROI delineations were determined,[17] and corticomedullary differences and ratios were calculated. Conventional T_1 mapping parameters included the mean cortical T_1 value (T_1-C), the mean medullary T_1 value (T_1-M), the mean corticomedullary difference [ΔT_1, (T_1-C) - (T_1-M)] and the mean corticomedullary ratio [T_1%, (T_1-C)/(T_1-M)].

Radiomics feature extraction

The radiomics features were extracted from the cortical ROIs on the native T_1 mapping images by using an open-resource Python package (Pyradiomics, version 3.9.1), and all extracted radiomics features conformed to the Image Biomarker Standardization Initiative (IBSI) standards. Four types of features (14 shape features, 18 first-order features, 75 original texture features and 744 wavelet features) were extracted for a total of 851 features. First, to ensure the consistency of the ROIs outlined by the two radiologists and to maintain the stability and reproducibility of the features, 30 lesions were randomly selected for secondary delineation, the extracted texture features were tested for reliability, and features with an intraclass correlation coefficient greater than 0.75 were considered reliable and reproducible and subsequently used for feature selection and model construction.

Radiomics feature selection and model construction

All features were normalized using the *Z* score (mean minus standard deviation) method before selection, which improved the stability of the data. After the reliability test, the least absolute shrinkage and selection operator (LASSO) regression was performed on the radiomics features of the training group for further data selection. For linear models, complexity was directly related to the number of variables in the model. The greater the number of variables, the more complex the model. More variables may give a seemingly better model when fitted, but at the same time there was a danger of overfitting. The LASSO regression algorithm performed a continuous penalized screening of all variables by means of a continuously imposed penalty term λ value. The larger λ penalized a linear model with more variables the stronger the penalty, thus ending up with a model with fewer variables in order to avoid covariance and overfitting. Therefore, LASSO regression was an effective method for identifying a larger number of variables with a smaller sample size. The LASSO regression algorithm performed a continuous penalized screening of all variables by means of a continuously imposed penalty term λ value, and a process whereby all characteristic variables continuously converge to zero. The features were then selected using 10-fold cross-validation method according to the criterion of least binomial deviance. For the final selection of non-zero features, multivariate logistic regression method was used to build classification and diagnosis model. To further illustrate the predictive value of the radiomics model in the classification and diagnosis of RF, we constructed

a combined model by integrating radiomics with clinical features. All processes involving the selection of texture features, construction and evaluation of diagnostic efficacy for the radiomics models were carried out using R software (version 4.1.1) and Python software (version 3.9.1).

Models comparison and validation

The diagnostic efficacy of all models was evaluated in terms of the area under the curve (AUC) of receiver operating characteristic (ROC). The accuracy of the models was calculated by means of confusion matrices, as well as sensitivity, specificity, positive predictive value and negative predictive value of each model. The calibration curve and Brier score were used to evaluate the calibration effect and goodness of fit of the radiomics model. The smaller the Brier score, the better the model fit and the closer the model was to the ideal model, the better the prediction performance of the model achieved. In addition, decision curve analysis (DCA) was used to evaluate the clinical effectiveness of models.

Clinical and laboratory parameters

Clinical characteristics, including age, gender, height, weight, body mass index (BMI), blood pressure, and blood glucose were collected for all patients. Laboratory parameters related to the kidney, including Scr, BUN and 24-h urinary protein (24h-UPRO) were also collected. The eGFR level was calculated based on Scr using the Chronic Kidney Disease Epidemiology Collaboration (CKD-EPI) equation.[3] CKD stages (G1-G5) were determined according to the Kidney Disease Outcomes Quality Initiative (K/DOQI) guidelines. In this study, patients were divided into three subgroups according to the values of eGFR: normal kidney function (abbreviated as KF 1) with CKD G1 (eGFR $\geq$90 mL/min/1.73m^2), mildly abnormal kidney function (abbreviated as KF 2) with CKD G2 (eGFR 60–89 mL/min/1.73m^2), and moderately to severely abnormal kidney function (abbreviated as KF 3) with CKD G3-5 (eGFR <60 mL/min/1.73m^2).

Renal histopathological evaluation

Ultrasound-guided renal biopsy was performed within 3 days post-MRI diagnosis. Renal biopsies were performed by two experienced nephrologists (X.Y. and Z.Y.), who were blinded to the MRI examination results. The patients were kept in the prone position, and a hard sandbag was placed under the abdomen to reduce the movement of the kidney during the puncture. In most cases, the bottom of the right kidney was the puncture site, and 16-gauge needles were used in this study.[33] Standard histopathological processing was performed on the renal biopsy tissue samples. RF was quantitatively assessed from the renal biopsy tissue sections by Masson's trichrome staining. RF was categorized as no RF (0% fibrosis), mild RF ($\leq$25% fibrosis), moderate RF (26%–50% fibrosis) and severe RF (>50% fibrosis).[34] In our study, patients with CKD were also divided into three subgroups: RF 1 (no RF), RF 2 (mild RF) and RF 3 (moderate RF and severe RF).

QUANTIFICATION AND STATISTICAL ANALYSIS

Statistical analyses were performed using R software version 4.1.1 (https://cran.r-project.org/), SPSS version 22.0 (https://www.ibm.com/products/spss-statistics) and MedCalc version 15.2.2 (https://medcalc.acadtechs.com/). Graphs were generated using GraphPad Prism 8 (http://www.graphpad-prism.cn). The Kolmogorov-Smirnov test or the Shapiro-Wilk test was used for normal distribution. Continuous variables with normal distribution were analyzed by paired or independent samples *t*-test and one-way analysis of variance (ANOVA) with Bonferroni correction, expressed as mean $\pm$ standard deviation. Categorical variables (frequencies and percentages) or continuous variables with nonnormal distribution [median (lower quartile, upper quartile)] were analyzed using Manni-Whitney U test, Wilcoxon signed-rank test or Kruskal-Wallis test. The intraclass correlation coefficient (ICC) was used to assess the inter-reader reproducibility between two radiologists with different experience. The ICC value ranges from 0 to 1 and is greater than 0.75, indicating good reliability. The Delong test was used to compare the diagnostic efficiency between the models. A two-tailed *p* value of less than 0.05 indicated statistical significance.